Wireless Powered IoE for 6G: Massive Access Meets Scalable Cell-Free Massive MIMO

Shuaifei Chen[1], Jiayi Zhang[1,*], Yu Jin[1], Bo Ai[2,3]

[1] School of Electronic and Information Engineering, Beijing Jiaotong University, Beijing 100044, China
[2] State Key Laboratory of Rail Traffic Control and Safety, Beijing Jiaotong University, Beijing 100044, China
[3] Henan Joint International Research Laboratory of Intelligent Networking and Data Analysis, Zhengzhou University, Zhengzhou 450001, China
* The corresponding author, email: jiayizhang@bjtu.edu.cn

Abstract: A key challenge to the scalable deployment of the energy self-sustainability (ESS) Internet of Everything (IoE) for sixth-generation (6G) networks is juggling massive connectivity and high spectral efficiency (SE). Cell-free massive multiple-input multiple-output (CF mMIMO) is considered as a promising solution, where many wireless access points perform coherent signal processing to jointly serve the users. However, massive connectivity and high SE are difficult to obtain at the same time because of the limited pilot resource. To solve this problem, we propose a new framework for ESS IoE networks where the user activity detection (UAD) and channel estimation are decoupled. A UAD detector based on deep convolutional neural networks, an initial access scheme, and a scalable power control policy are proposed to enable the practical scalable CF mMIMO implementation. We derive novel and exact closed-form expressions of harvested energy and SE with maximum ratio (MR) processing. Using local partial minimum mean-square error and MR combining, simulation results prove that the proposed framework can serve more users, improve the SE performance, and achieve better user fairness for the considered ESS IoE networks.

Keywords: 6G network; cell-free massive MIMO; energy self-sustainability; Internet of Everything

Received: Jul. 9, 2020
Revised: Aug. 30, 2020
Editor: Kun Yang

I. INTRODUCTION

While fifth-generation (5G) is being commercially deployed worldwide, research into sixth-generation (6G) is started, which is expected to include energy self-sustainability (ESS) Internet of Everything (IoE) networks [1-4]; that is handling a significantly massive connectivity and delivering huge amounts of data traffic, while providing a more uniform quality-of-service (QoS) throughout the entire wireless network [5].

Cellular massive multiple-input multiple-output (MIMO) is recognized as a component of the 5G networks [6][8]. With inheriting several virtues from cellular massive MIMO (in particularly *favorable propagation*), cell-free massive MIMO (CF mMIMO) [9-12] is considered to potentially reach the requirements of ESS IoE networks in 6G (for instance, strong macro-diversity and ubiquitous coverage). The basic idea of CF mMIMO is that a large number of wireless access points (APs), which could be arbitrarily distributed in the coverage area and connected to a central processing unit (CPU), jointly serve all user equipments (UEs) on the same time-frequency resource under the coordination and computational assistance from the CPU [13-16]. Hence, CF mMIMO can be viewed as an enabler to massive access for the following two features. Firstly, its macro-diversity could greatly improve the coverage probability compared with cellular technology [9], [10], [14]. Secondly, interference is managed by having a user-centric subset of the APs serve each user [17-19]. These two features allow CF mMIMO to accommodate more UEs than cellular networks, where inter-cell interference and pilot shortage are the limiting factors. Note that CF mMIMO is a practically implementable evolution of coordinated multipoint (CoMP) [20, Sec. 7.4.3], where the APs form joint clusters instead of disjoint clusters which act as cells in the sense that the APs in a cluster can be treated as a “federated base station”.

An ESS network can be implemented by wireless power transfer (WPT), where the ambient and dedicated radio frequency (RF) energy is harvested for the battery-limited UEs [21-23]. Time-switching protocol is well considered in WPT cellular massive MIMO operating in time division duplex (TDD) mode [24], where the transmission interval is divided into slots for energy harvest and information reception. The rationale behind integrating CF mMIMO with WPT is that each UE can be served by at least one AP with stronger channel gain compared with cellular technology, which makes WPT feasible in the dense scenarios.

Although the benefits of CF mMIMO over cellular massive MIMO are well established, it will still be two challenges to practically exploit CF mMIMO in ESS IoE networks. One is juggling massive connectivity and high spectral efficiency. Due to the pilot shortage, non-orthogonal pilots [25] or orthogonal hopping pilots [26] are normally used for the massive user activity detection (UAD) and channel estimation (CE). However, these joint UAD and CE schemes achieve massive connectivity with the penalty of the inaccuracy of the channel state information (CSI), which makes coherent transmission less effective and hence deteriorates the throughput performance. Especially in the considered WPT scenarios, the energy used for uplink payload transmission is harvested from WPT, which is closely depends on the accuracy of the CSI acquired by channel estimation. In this paper, we propose to decouple the user identifiers and pilot sequence. Exclusive non-orthogonal identifiers for each UEs are utilized for UAD and orthogonal pilots are assigned to the detected active UEs for CE during the transmission. The other challenge is the scalable implementation which was first considered in [18], where the authors declare that a CF mMIMO network should guarantee the complexity and resource requirements of signal processing to be finite for each AP as the number of active UEs approaches to infinity. Although several algorithms for initial access and power control in CF mMIMO have been proposed in [18], it was not designed for massive access scenario and won’t perform well in this case. Hence, the main objective of this paper is to design a framework for juggling massive access and high spectral efficiency by exploiting CF mMIMO in EES IoE networks.

We proposed a framework comprising a CNN-based user activity detector, an initial access scheme which jointly performs AP selection and pilot assignment, and a scalable power control policy considering both uplink and downlink.

1.1 Related works

There are a large body of works} on massive access in cellular massive MIMO [25-30]. Authors in [25] utilized non-orthogonal pilots for UAD and CE in a massive machine-type communication (MTC) scenario by exploiting compressive sensing. In [26], the authors improved the random access performance by averaging the pilot contamination across the transmission slots with pilot hopping. The authors in [27] proposed a non-Bayesian algorithm to detect the activity of a large number of UEs for massive unsorted random access. However, due to the sporadic nature of the transmission in IoE scenarios, the system can dedicate the resources (pilot, computation, etc.) to the active UEs given they are detected, in order to achieve higher data rates.

CF mMIMO was proposed in [9], [10], but

builds on the heritage of CoMP. In [14], the signal processing between the APs and CPU is divided into four different modes. The most promising distributed implementation utilized minimum mean-squared-error (MMSE) combining along with large-scale fading decoding (LSFD) [31]. Although all APs initially served all UEs, the user-centric approach has become the leading manner to achieve a practically implementation [17-19]. The existing works on WPT on CF mMIMO are limited [32-34]. Authors in[32] considered WPT in a CF mMIMO where the UEs were separated into the ones for information and the ones for energy. In [33], the authors minimized the total transmitted energy of wireless-powered cell-free Internet of Things (IoT) networks by considering uncorrelated Rayleigh channel fading. In [34], a max-min fairness power control was considered for WPT with CF mMIMO where the channel was modeled as uncorrelated Rician fading. The initial access in CF mMIMO is considered in [8], [18], [19], [35], [36]. Schemes based on greedy algorithm and tabu-search were provided in [9] and [35], respectively. Both of the them are not scalable. In [18], a scalable scheme was performed by individually providing each accessing UE with the least bad pilot and allocating each accessing UE with at least on AP. Delicate initial access algorithms based on user-clustering were proposed in [19]. However, those algorithms are heuristic and complex, hence not suitable for the considered IoE scenarios.

1.2 Main contributions

In this paper, we design a massive access framework for juggling massive access and high spectral efficiency by exploiting CF mMIMO in EES IoE networks. Our main contributions are given as follows.

1) We decouple the UE identifier and pilot sequences, and propose a UAD convolutional neural network (UADNet) which achieves an excellent detection performance compared with our proposed simple benchmark wherein the received identifier power is utilized.
2) We propose a scalable initial access scheme based on a competitive mechanism which jointly assigns a large number of active UEs with appropriate pilots and APs for service.
3) We propose a scalable power control policy which makes the best use of the harvested energy to obtain a suitable tradeoff between fairness and average SE by adjusting a parameter.
4) We derive two novel closed-form expressions for harvested energy with maximum ratio (MR) precoding and spectral efficiency (SE) with MR combining, respectively. These expressions are suitable for arbitrarily fixed pilot assignment schemes.

1.3 Paper outline and notations

The remainder of this paper is organized as follows. Section II introduces the system model for ESS IoE CF mMIMO. Section III elaborates the transmission procedure, including the closed-form expressions for harvested energy and SE, and the scalable power control policy. User activity detectors based on convolutional neural networks (CNN) and received identifier power and initial access scheme are proposed in Section IV and Section V, respectively. The performance of the proposed massive access framework is numerically evaluated in Section VI. Finally, the major conclusions and implications are drawn in Section VII.

Boldface lowercase letters, $\mathbf{x}$, denote column vectors and boldface uppercase letters, $\mathbf{X}$, denote matrices. The superscripts $^{\mathrm{T}}$, *, and $^{\mathrm{H}}$ denote transpose, conjugate, and conjugate transpose, respectively. We use $\triangleq$ for definitions and $\mathrm{diag}\left(a_1,\ldots,a_n\right)$ for a diagonal matrix with elements $a_1,\ldots,a_n$ on the diagonal. The multi-variate circularly symmetric complex Gaussian distribution with correlation matrix $\mathbf{R}$ is denoted $\mathcal{N}_{\mathbb{C}}\left(\mathbf{0},\mathbf{R}\right)$. The expected value of $\mathbf{x}$ is denoted as $\mathbb{E}\left\{\mathbf{x}\right\}$. We denote by $\left\|\mathbf{x}\right\|_2$ the Euclidean norm of $\mathbf{x}$. We use $\left|\mathcal{A}\right|$ and $\left[\mathcal{A}\right]_n$ to denote the cardinality and the n th element of the set $\mathcal{A}$, respectively.

II. System Model

We consider a CF mMIMO system consisting of K single-antenna wireless powered UEs and L APs equipped with N antennas. As illustrated in Figure 1(a), all APs are connected to a CPU in an arbitrary fashion. We assume that the fronthaul connections are error-free since the focus of this paper is not on fronthaul provisioning. The channel between AP l and UE k is denoted as $\mathbf{h}_{kl} \in \mathbb{C}^N$ The standard block fading model is considered [20], where $\mathbf{h}_{kl}$ is constant in time-frequency intervals of τ_c channel uses. In each interval, an independent realization from a correlated Rayleigh fading distribution is drawn as $\mathbf{h}_{kl} \sim \mathcal{N}_{\mathbb{C}}(\mathbf{0}, \mathbf{R}_{kl})$, where $\mathbf{R}_{kl}$ is the spatial correlation matrix describing the spatial property of the channel, and $\beta_{kl} \triangleq \mathrm{tr}(\mathbf{R}_{kl})/N$ is the large-scale fading coefficient that describes pathloss and shadowing. The fading channels of different links are independently distributed. We assume that deterministic information is known to the system; in particular, the spatial correlation matrices $\{\mathbf{R}_{kl}\}$ are available at the APs and the geographic locations of the APs are available at the CPU. For concise description, we denote by $\mathcal{M}_k$ the subset of APs serving UE k, and $\mathcal{D}_l$ the subset of UEs served by AP l.

The IoE scenario is considered, in which the number of the UEs, i.e., K is tremendously large. Among these UEs, only a relatively small number of UEs stay active with activation probability ϵ when they have payload data to transmit, otherwise, they remain idle to save energy. We assume the system is operating in TDD mode, and then the channel reciprocity holds. As illustrated in Figure 1(b), the transmission is organized into transmission frames consisting of multiple coherence intervals, where each coherence interval is divided into three phases: τ_p channel uses for uplink CE, τ_d channel uses for downlink energy harvest, and τ_u channel uses for uplink data transmission such that $\tau_c = \tau_p + \tau_d + \tau_u$. Moreover, we denote by $\lambda = \tau_d / (\tau_c - \tau_p)$ the time switch ratio which dynamically allocates channel uses for energy and data. Unlike the works in the context of MTC/IoT scenarios where user activity detection (UAD) is coupled with CE to the pilot sequences [37], we decouple UAD and CE by having τ_i channel uses dedicated for UAD once a UE is activated and having τ_p channel uses for CE in each of the following coherence intervals. We denote by $\{\boldsymbol{\varphi}_t : t = 1, \ldots, \tau_p\}$ the pilot set consisting of τ_p *mutually orthogonal* τ_p-length pilot sequences with $\|\boldsymbol{\varphi}_t\|^2 = \tau_p$, and denote by $\{\phi_k : k = 1, \ldots, K\}$ the identifier set consisting of K *non-orthogonal* τ_i-length identifier sequences with $\|\phi_k\|^2 = \tau_i$.

When a UE k is activated, it first broadcasts its identifier ϕ_k so that the system can be aware of its presence by UAD, which is elaborated in Section IV. Then, the system assigns UE k a pilot $\boldsymbol{\varphi}_t$ and at least an AP as its serving AP by performing AP selection and pilot assignment, which is elaborated in Section V. Finally, the transmission between UE k and its serving

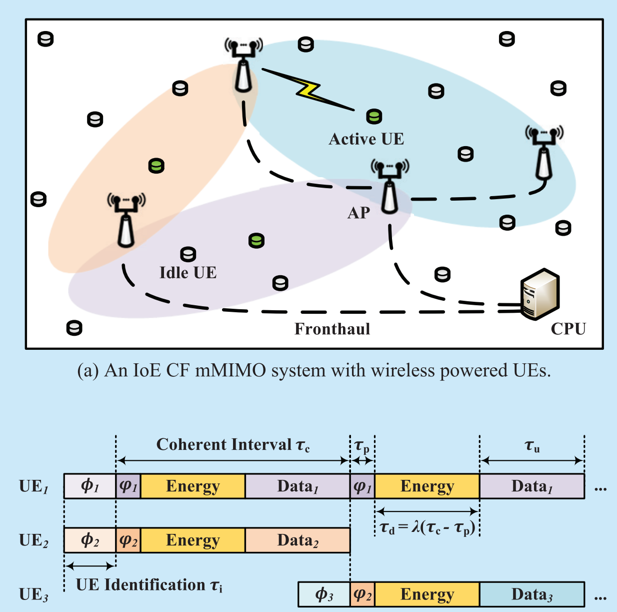

(a) An IoE CF mMIMO system with wireless powered UEs.

(b) Transmission structure.

Fig. 1. *Illustration for the considered wireless powered IoE CF mMIMO systems, where only a relatively small number of UEs stay active with activation probability* ϵ.

APs commences, in which i) UE k transmits $\boldsymbol{\varphi}_t$ for CE, ii) serving APs transmit the precoded energy signal based on the CSI, and iii) UE k transmits its payload data with the harvested energy. Since the transmission is sporadic, $\boldsymbol{\varphi}_t$ will be released for the new active UEs when UE k's transmission ends (see next Section for detail).

III. Coherent Transmission and Spectral Efficiency

Pilot-based coherent transmission is essential for a multiple antenna system, especially when WPT is considered [34]. The rationale behind this is that the energy used for uplink payload transmission is harvested from WPT, which is largely depends on the CSI acquired by pilot training. In this section, we analyze the SE performance of our proposed ESS IoT CF mMIMO system with coherent transmission given the active UEs are detected. We denote by $\mathcal{K} \subset \{1,\ldots,K\}$ the subset of the active UEs in the system. Closed-form expressions for the average harvested energy and SE with simple MR procoding and MR combining are derived in order to offer insights of the system. A simple scalable power control policy is given at the end of this section.

3.1 Pilot training and channel estimation

The pilots $\{\boldsymbol{\varphi}_t\}$ are assigned to the active UEs when they access the system by exploiting the joint AP selection and pilot assignment schemes proposed in Section V. Although we only deal with the signal processing of the active UEs with an activation probability $\epsilon \sim 0.01, |\mathcal{K}| > \tau_p$ is assumed since K is tremendously large in the considered IoE scenarios. Hence, several UEs share the same pilot. For now, we denote by $\mathcal{S}_t \subset \mathcal{K}$ the subset of UEs sharing $\boldsymbol{\varphi}_t$. When these UEs in $\mathcal{S}_t$ transmit $\boldsymbol{\varphi}_t$, AP l receives the pilot signal $\mathbf{y}_{tl}^{\mathrm{p}} \in \mathbb{C}^N$ as [20, Sec. 3]

$$\mathbf{y}_{tl}^{\mathrm{p}} = \sum_{i \in \mathcal{S}_t} \sqrt{\tau_p \rho_p} \mathbf{h}_{il} + \mathbf{n}_{tl}, \tag{1}$$

where ρ_p dentes the pilot transmit power of UE i and $\mathbf{n}_{tl} \sim N_{\mathbb{C}}\left(\mathbf{0}, \sigma^2 \mathbf{I}_N\right)$ is the thermal noise. The MMSE estimate of $\mathbf{h}_{kl}$ for $k \in \mathcal{S}_t$ is given by [20, Sec. 3]

$$\hat{\mathbf{h}}_{kl} = \sqrt{\tau_p \rho_p} \mathbf{R}_{kl} \mathbf{\Psi}_{tl}^{-1} \mathbf{y}_{tl}^{\mathrm{p}}, \tag{2}$$

where

$$\mathbf{\Psi}_{tl} = \mathbb{E}\left\{\mathbf{y}_{tl}^{\mathrm{p}} \left(\mathbf{y}_{tl}^{\mathrm{p}}\right)^{\mathrm{H}}\right\} = \sum_{i \in \mathcal{S}_t} \tau_p \rho_p \mathbf{R}_{kl} + \sigma^2 \mathbf{I}_N \tag{3}$$

is the correlation matrix of . The estimate $\hat{\mathbf{h}}_{kl}$ and estimation error $\tilde{\mathbf{h}}_{kl} = \mathbf{h}_{kl} - \hat{\mathbf{h}}_{kl}$ are independent vectors distributed as $\hat{\mathbf{h}}_{kl} \sim \mathcal{N}_{\mathbb{C}}\left(\mathbf{0}, \mathbf{B}_{kl}\right)$ and $\tilde{\mathbf{h}}_{kl} \sim \mathcal{N}_{\mathbb{C}}\left(\mathbf{0}, \mathbf{C}_{kl}\right)$, where

$$\mathbf{B}_{kl} = \mathbb{E}\left\{\hat{\mathbf{h}}_{kl} \hat{\mathbf{h}}_{kl}^{\mathrm{H}}\right\} = \tau_p \rho_p \mathbf{R}_{kl} \mathbf{\Psi}_{tl}^{-1} \mathbf{R}_{kl}, \tag{4}$$

$$\mathbf{C}_{kl} = \mathbb{E}\left\{\tilde{\mathbf{h}}_{kl} \tilde{\mathbf{h}}_{kl}^{\mathrm{H}}\right\} = \mathbf{R}_{kl} - \mathbf{B}_{kl}. \tag{5}$$

Note that indicates that sharing pilot $\boldsymbol{\varphi}_t$ among the UEs in $\mathcal{S}_t$ generates mutual interference, and consequently degrades the system performance, which is the so-called *pilot contamination*.

3.2 Downlink energy transmission

During the downlink energy transmission, the coherent fashion is considered where all APs synchronously transmit the same energy signal for their serving UEs in order to harvest more energy at UEs. We denote by $\mathbf{w}_{il} = \frac{\bar{\mathbf{w}}_{il}}{\sqrt{\mathbb{E}\left\{\|\bar{\mathbf{w}}_{il}\|^2\right\}}}$ the normalized precoder that AP l assigns to UE i, where $\mathbb{E}\left\{\|\mathbf{w}_{il}\|^2\right\} = 1$. Then the received signal at UE k is

$$e_k = \sum_{l=1}^{L} \mathbf{h}_{kl}^{\mathrm{T}} \sum_{i \in \mathcal{K}} \sqrt{\eta_{il}} \mathbf{w}_{il}^{*} q_i + n_k, \tag{6}$$

where $q_i \in \mathbb{C}$ is zero-mean unit-variance energy signal for UE i, $\eta_{il} \geqslant 0$ is the power control coefficient of AP l and UE i, and $n_k \sim \mathcal{N}_{\mathbb{C}}\left(0, \sigma^2\right)$ is the receiver noise. The transmission power of each AP should be upper bounded by the maximum power ρ_d, i.e.,

$$\mathbb{E}\left\{\left\|\sum_{i\in\mathcal{K}}\sqrt{\eta_{il}}\mathbf{w}_{il}^{*}q_i\right\|^2\right\}=\sum_{i\in\mathcal{K}}\eta_{il}\leqslant\rho_d. \quad (7)$$

Since the noise floor is trivial for energy harvest, we adopt the operation from the existing literature [32], [34] that simply neglecting the effect of n_k in the expression for the average harvested energy.

Lemma 1. *The average harvested energy for UE k of cell-free massive MIMO is given as*

$$\begin{aligned}\mathcal{E}_k&=\mathbb{E}\left\{\left|\sum_{l=1}^{L}\sum_{i\in\mathcal{K}}\sqrt{\eta_{il}}\mathbf{w}_{il}^{\mathrm{H}}\mathbf{h}_{kl}q_i\right|^2\right\}\\&=\sum_{l=1}^{L}\sum_{j=1}^{L}\sum_{i\in\mathcal{K}}\sqrt{\frac{\eta_{il}\eta_{ij}}{\mathbb{E}\left\{\left\|\bar{\mathbf{w}}_{il}\right\|^2\right\}\mathbb{E}\left\{\left\|\bar{\mathbf{w}}_{ij}\right\|^2\right\}}}\\&\quad\times\mathbb{E}\left\{\bar{\mathbf{w}}_{il}^{\mathrm{H}}\mathbf{h}_{kl}\mathbf{h}_{ij}^{\mathrm{H}}\bar{\mathbf{w}}_{kj}\right\},\end{aligned}\quad (8)$$

where the expectations are with respect to all sources of randomness.

Proof: It follows the fact that the energy signals and the channels of different APs are independent.

Any precoder can be adopted in the above expression. By considering the simple MR precoding, we can obtain the following closed-form expression as a simple baseline which offers insights of the system.

Lemma 2. *If MR precoder $\bar{\mathbf{w}}_{il}=\hat{\mathbf{h}}_{il}$ is used, the average harvested energy for UE k, i.e., $\mathcal{E}_k$ in (8) becomes*

$$\begin{aligned}\mathcal{E}_k&=\sum_{l=1}^{L}\sum_{i\in\mathcal{K}}\frac{\eta_{il}}{\mathrm{tr}\left(\mathbf{B}_{il}\right)}\mathbb{E}\left\{\bar{\mathbf{w}}_{il}^{\mathrm{H}}\mathbf{h}_{kl}\mathbf{h}_{kl}^{\mathrm{H}}\bar{\mathbf{w}}_{il}\right\}\\&\quad+\sum_{l=1}^{L}\sum_{j=1,j\neq i}^{L}\sum_{i\in\mathcal{K}}\sqrt{\frac{\eta_{il}\eta_{ij}}{\mathrm{tr}\left(\mathbf{B}_{il}\right)\mathrm{tr}\left(\mathbf{B}_{ij}\right)}}\\&\quad\times\mathbb{E}\left\{\bar{\mathbf{w}}_{il}^{\mathrm{H}}\mathbf{h}_{kl}\right\}\mathbb{E}\left\{\mathbf{h}_{kj}^{\mathrm{H}}\bar{\mathbf{w}}_{ij}\right\}\end{aligned}\quad (9)$$

$$\begin{aligned}&=\sum_{l=1}^{L}\sum_{i\in\mathcal{K}}\eta_{il}\frac{\mathrm{tr}\left(\mathbf{B}_{il}\mathbf{R}_{kl}\right)}{\mathrm{tr}\left(\mathbf{B}_{il}\right)}\\&\quad+1_{\{\boldsymbol{\varphi}_i=\boldsymbol{\varphi}_k\}}\left|\sum_{l=1}^{L}\sum_{i\in\mathcal{K}}\sqrt{\eta_{il}}\frac{\mathrm{tr}\left(\mathbf{B}_{il}\mathbf{R}_{il}^{-1}\mathbf{R}_{kl}\right)}{\sqrt{\mathrm{tr}\left(\mathbf{B}_{il}\right)}}\right|^2\end{aligned}\quad (10)$$

where $1_{\{\cdot\}}$ is the indicator function, i.e., $1_{\{\boldsymbol{\varphi}_i=\boldsymbol{\varphi}_k\}}$ is 1 if $\boldsymbol{\varphi}_i=\boldsymbol{\varphi}_k$ and 0 otherwise.

Proof: It follows the standard expectations and hence omitted due to space limitation.

Note that the second term in (9) disappears when the non-coherent energy transmission is considered, where no synchronization is needed among APs and hence each AP is allowed to make their choice of energy signals to transmit. Since all terms in (9) are opposite, it is easy to tell that the coherent energy transmission can always offer more harvested energy at UEs. From (10) we can see that all signals from all APs, including the desired signal and the interference signal intended to other UEs, make a contribution to the harvested energy. Moreover, the second term in (10) comes from the pilot contamination which reduces the channel estimation quality on one hand, and does bring some additional energy on the other. Hence it is not easy to tell from the above expression if the pilot contamination increases the harvested energy or not.

3.3 Uplink data transmission

During the uplink data transmission, AP l receives the signal $\mathbf{y}_l\in\mathbb{C}^N$ from all UEs, as

$$\mathrm{y}_l=\sum_{i\in\mathcal{K}}\sqrt{p_i}\mathbf{h}_{il}s_i+\mathbf{n}_l, \quad (11)$$

where $s_i\sim\mathcal{N}_{\mathbb{C}}\left(0,1\right)$ is the signal transmitted from UE i with power p_i, and $\mathbf{n}_l\sim\mathcal{N}_{\mathbb{C}}\left(\mathbf{0},\sigma^2\mathbf{I}_N\right)$ is the independent receiver noise.

For the large-scale network deployment, we prefer to offload most of the computational tasks to the APs to avoid overloading the CPU. More specifically, every AP preprocesses its signal by computing local estimates of the data and then passes them to the CPU for final decoding, which is the so-called *LSFD*. We denote by $\mathbf{v}_{kl}\in\mathbb{C}^N$ the combining vector selected by AP l for UE k. Then, the local estimate of s_k is given by

$$\tilde{s}_{kl}=\mathbf{v}_{kl}^{\mathrm{H}}\mathrm{y}_l=\sum_{i\in\mathcal{K}}\sqrt{p_i}\mathbf{v}_{kl}^{\mathrm{H}}\mathbf{h}_{il}s_i+\mathbf{v}_{kl}^{\mathrm{H}}\mathbf{n}_l. \quad (12)$$

Any combining vector can be adopted in the above expression.

The simple MR combining with $\mathbf{v}_{kl}^{\mathrm{MR}}=\hat{\mathbf{h}}_{kl}$ was considered in [31], while [18] has recently advocated for using the local partial MMSE (LP-MMSE) combining

$$\mathbf{v}_{kl}^{\text{LP-MMSE}} = p_k \left(\sum_{i\in\mathcal{D}_l} p_i \left(\hat{\mathbf{h}}_{il}\hat{\mathbf{h}}_{il}^{\text{H}} + \mathbf{C}_{il} \right) + \sigma^2 \mathbf{I}_N \right)^{-1} \hat{\mathbf{h}}_{kl}. \tag{13}$$

Then the local estimates $\{\tilde{s}_{kl}\}$ are sent to the CPU, where they are linearly combined by using the weights $\{a_{kl}\}$ to obtain $\hat{s}_k = \sum_{l=1}^{L} a_{kl}^* \tilde{s}_{kl}$, which is eventually used to decode s_k. From (12), we have the final estimate of s_k, as

$$\begin{aligned} \hat{s}_k &= \sum_{l=1}^{L} \sqrt{p_k} a_{kl}^* \mathbf{v}_{kl}^{\text{H}} \mathbf{h}_{kl} s_k \\ &+ \sum_{l=1}^{L} \sum_{i\in\mathcal{K}, i\neq k} \sqrt{p_i} a_{kl}^* \mathbf{v}_{kl}^{\text{H}} \mathbf{h}_{il} s_i + \sum_{l=1}^{L} a_{kl}^* \mathbf{v}_{kl}^{\text{H}} \mathbf{n}_l. \end{aligned} \tag{14}$$

Since the CPU does not have the knowledge of channel estimates, we utilize the so-called *use-and-then-forget* (UatF) bound [20, The. 4.4] to obtain the achievable SE.

Lemma 3. *The achievable SE for UE k of cell-free massive MIMO is*

$$\text{SE}_k = \left(\frac{\tau_u}{\tau_c} \right) \log_2 \left(1 + \text{SINR}_k \right), \tag{15}$$

where the signal-to-interference-and-noise ratio (*SINR*) *is given by*

$$\text{SINR}_k = \frac{p_k \left| \mathbf{a}_k^{\text{H}} \mathbf{u}_k \right|^2}{\mathbf{a}_k^{\text{H}} \left(\sum_{i\in\mathcal{K}} p_i \mathbf{\Lambda}_{ki}^{(1)} - p_k \mathbf{u}_k \mathbf{u}_k^{\text{H}} + \sigma^2 \mathbf{\Lambda}_k^{(2)} \right) \mathbf{a}_k},$$

where

$$\mathbf{a}_k = \left[a_{k1}, \ldots, a_{kL} \right]^{\text{T}}, \tag{16}$$

$$\mathbf{u}_k = \left[\mathbb{E}\left\{ \mathbf{v}_{k1}^{\text{H}} \mathbf{h}_{k1} \right\}, \ldots, \mathbb{E}\left\{ \mathbf{v}_{kL}^{\text{H}} \mathbf{h}_{kL} \right\} \right]^{\text{T}}, \tag{17}$$

$$\mathbf{\Lambda}_{ki}^{(1)} = \left[\mathbb{E}\left\{ \mathbf{v}_{kl}^{\text{H}} \mathbf{h}_{il} \mathbf{h}_{ij}^{\text{H}} \mathbf{v}_{kj} \right\} : l, j = 1, \ldots, L \right], \tag{18}$$

$$\mathbf{\Lambda}_k^{(2)} = \text{diag}\left(\mathbb{E}\left\{ \|\mathbf{v}_{k1}\|^2 \right\}, \ldots \mathbb{E}\left\{ \|\mathbf{v}_{kL}\|^2 \right\} \right), \tag{19}$$

and the expectations are with respect to all sources of randomness.

Proof: It follows the similar approach as in [20, The. 4.4], but for the received signal in (14).

The structure of (16) is a generalized Rayleigh quotient with respect to $\mathbf{w}_k$. As a consequence, the maximum value of SINR_k is achieved with the optimal LSFD weight [20, Lem. B.10]

$$\mathbf{w}_k^{\text{LSFD}} = \left(\sum_{i=1}^{K} p_i \mathbf{\Lambda}_{ki}^{(1)} + \sigma^2 \mathbf{\Lambda}_k^{(2)} \right)^{-1} \mathbf{v}_k. \tag{20}$$

However, the implementation of the optimal LSFD in (20) is unscalable due to the unbounded fronthaul load and computational complexity as $K \to \infty$. An alternative Partial LSFD (P-LSFD) is proposed in [19] to achieve scalable implementation with insignificant sacrifice of performance loss, as

$$\mathbf{w}_k^{\text{P-LSFD}} = \left(\sum_{i\in\mathcal{R}_k} p_i \mathbf{\Lambda}_{ki}^{(1)} + \sigma^2 \mathbf{\Lambda}_k^{(2)} \right)^{-1} \mathbf{v}_k, \tag{21}$$

where $\mathcal{R}_k = \{ i : \mathcal{M}_k \cap \mathcal{M}_i \neq \varnothing \}$ is the subset of the UEs which are served by partially the same APs as UE k. Only those UEs in $\mathcal{R}_k$ might cause substantial interference to UE k.

The expectations in Lemma 3 cannot be computed in closed-form when using LP-MMSE, but can be easily computed using Monte-Carlo simulations. Similar to [20, Cor. 4.5], we can obtain the following closed-form expression as a simple baseline when using MR combining.

Lemma 4. *If MR combining with* $\mathbf{a}_{kl}^{\text{MR}} = \hat{\mathbf{h}}_{kl}$ *is used*, *the expectations in Lemma* 3 *become*

$$\mathbb{E}\left\{ \mathbf{v}_{kl}^{\text{H}} \mathbf{h}_{kl} \right\} = \text{tr}\left(\mathbf{B}_{kl} \right), \tag{22}$$

$$\mathbb{E}\left\{ \|\mathbf{v}_{kl}\|^2 \right\} = \text{tr}\left(\mathbf{B}_{kl} \right), \tag{23}$$

and

$$\mathbb{E}\left\{ \mathbf{v}_{kl}^{\text{H}} \mathbf{h}_{il} \mathbf{h}_{ij}^{\text{H}} \mathbf{v}_{kj} \right\} = \begin{cases} \text{tr}\left(\mathbf{B}_{kl} \mathbf{R}_{il} \right) + 1_{\{\boldsymbol{\varphi}_i = \boldsymbol{\varphi}_k\}} \left| \text{tr}\left(\mathbf{B}_{kl} \mathbf{R}_{kl}^{-1} \mathbf{R}_{il} \right) \right|^2 & \text{if } j = l, \\ 1_{\{\boldsymbol{\varphi}_i = \boldsymbol{\varphi}_k\}} \text{tr}\left(\mathbf{B}_{kl} \mathbf{R}_{kl}^{-1} \mathbf{R}_{il} \right) \text{tr}\left(\mathbf{B}_{kj} \mathbf{R}_{kj}^{-1} \mathbf{R}_{ij} \right) & \text{otherwise.} \end{cases} \tag{24}$$

Proof: It follows the similar approach as in [20, Cor. 4.5], but for the received signal in (14).

3.4 Scalable power control

Since the UEs in the considered system are assumed to be ESS, the total energy required for uplink pilot and payload data transmission is upper bounded by the total harvested energy E_k for UE k, i.e.,

$$\tau_p \rho_p + \tau_u \rho_{u,k} = E_k, \tag{25}$$

where $\rho_{u,k}$ is the maximum uplink transmit power of UE k.

The linear energy harvest model is adopted [33], hence the total harvested energy at UE k during τ_d channel uses is

$$E_k = \tau_d \xi \mathcal{E}_k \left(\left\{\eta_{ij}\right\}\right), \tag{26}$$

where $\xi \in [0,1]$ is the RF-to-DC conversion efficiency. Note that the average harvested energy is a linear function of the downlink power control coefficients $\{\eta_{ij}\}$.

For the scalable downlink precoding, we adopt the power control policy from [18]

$$\eta_{kl} = \begin{cases} \dfrac{\sqrt{\beta_{kl}}}{\sum_{i \in D_l} \sqrt{\beta_{il}}} \rho_d & \text{if } k \in \mathcal{D}_l \\ 0 & \text{otherwise,} \end{cases} \tag{27}$$

where AP l only transmits energy signal to the UEs in $\mathcal{D}_l$.

For the scalable uplink combining, we follow the fractional power control policy from [19]

$$p_k = \frac{\min_i \left(\sum_{l \in M_i} \beta_{il}\right)^{\theta}}{\left(\sum_{l \in M_k} \beta_{kl}\right)^{\theta}} \rho_{u,k}, \tag{28}$$

where $\theta \in [0,1]$ indicates how much the received powers is compressed. Larger values of θ promote more fairness and $\theta = 0$ is the so-called *equal power allocation* or *full power transmission*.

It is worth noting that the downlink and uplink power control policy are designed by the principle that an AP l only serves the UEs in $\mathcal{D}_l$, which prevents the fronthaul load and the computation complexity from being unbounded as $|\mathcal{K}| \to \infty$, and hence makes the considered system implementation scalable.

IV. USER ACTIVITY DETECTION

When a UE k has data to transmit, it first broadcasts its exclusive identifier ϕ_k so that the APs in the system are aware of its presence. In this section, we first propose a simple detection method based on the received identifier signal power as a benchmark. Then we propose a UADNet, where the CNN is widely utilized in classification and detection [38], [39]. The motivation of UADNet comes from the higher detection accuracy or lower online computation complexity compared with the conventional methods like the proposed benchmark or compressive sensing [25].

4.1 Non-orthogonal identifier sequences

Due to the natural channel variations in time and frequency domain, exclusive orthogonal identifiers are infeasible for the IoE scenarios, which leads us to non-orthogonal identifiers. We use the simple combinatorial number to construct identifiers since the focus of this paper is not on identifier design. Recall that UE k's identifier is denoted by $\phi_k \triangleq \sqrt{\frac{\tau_i}{m}} \left[\phi_{k1}, \ldots, \phi_{k\tau_i}\right]^{\mathrm{T}} \in \mathbb{C}^{\tau_i}$, where $\tau_i \leqslant \tau_c$. Among the τ_i elements in ϕ_k, m of the them are selected to be 1, the others are 0, which implies $\sum_{n=1}^{\tau_i} \phi_{kn} = m$. Hence, there are $C(\tau_i, m)$ unique identifiers, where $C(n,k)$ is the combinatorial number corresponds to taking k -combinations from the set of size n. The above description implies that the non-orthogonal identifier sequences could be generated by sampling an independent and identically (i.i.d.) Bernoulli distribution, where the probability of $\phi_{kn} = 1$ is $\frac{m}{\tau_i}$, and $1 - \frac{m}{\tau_i}$ otherwise.

Once a UE broadcasts it identifier sequence, the APs jointly performs UAD based on their received identifier signal, which is elaborated in following Subsections.

4.2 Power-based approach

Similar to the pilot signal $\mathbf{y}_{tl}^{\mathrm{p}} \in \mathbb{C}^N$ in (1), AP l received the identifier signal $\mathbf{y}_{kl}^{\mathrm{i}} \in \mathbb{C}^N$ as

$$\begin{aligned}\mathbf{y}_{kl}^{\mathrm{i}} &= \sqrt{\frac{\rho_i}{\tau_i}} \sum_{k'=1}^{K} \delta_{k'} \mathbf{h}_{k'l} \phi_{k'}^{\mathrm{T}} \phi_k^* + \mathbf{n}_{kl} \\ &\overset{(a)}{=} \sqrt{\tau_i \rho_i} \sum_{k'=1}^{K} \delta_{k'} \mathbf{h}_{k'l} \frac{\hat{m}_{k'}}{m} + \mathbf{n}_{kl}\end{aligned} \tag{29}$$

where $\delta_{k'}$ indicates whether UE k' is active or not, i.e., $\delta_{k'} = 1$ means UE k' is active, and $\delta_{k'} = 0$ otherwise.

ρ_i denotes the identifier transmit power of UE k' and $\mathbf{n}_{kl} \sim \mathcal{N}_{\mathbb{C}}\left(\mathbf{0}, \sigma^2 \mathbf{I}_N\right)$ is the thermal noise. (a) comes from the fact that $\phi_{k'}^{\mathrm{T}} \phi_k^* = \tau_i \frac{\hat{m}_{k'}}{m}$, where the integer $\hat{m}_{k'} = m$ if $k' = k$, and $\hat{m}_{k'} = 1, \ldots, m-1$ otherwise. Then, all APs (through the CPU) jointly make a calculation of

$$\begin{aligned}\mathcal{Y} &\triangleq \sum_{l=1}^{L} \operatorname{tr}\left(\mathbb{E}_{\{\mathbf{h}\}}\left\{\left\|\mathbf{y}_{kl}^{\mathrm{i}}\right\|^2\right\}\right) \\ &= \tau_i \rho_i \sum_{l=1}^{L} \beta_{kl} + \tau_i \rho_i \sum_{l=1}^{L} \sum_{k'=1, k' \neq k}^{K} \delta_{k'} \beta_{k'l} \left(\frac{\hat{m}_{k'}}{m}\right)^2 + L\sigma^2\end{aligned} \tag{30}$$

to check the UE k's presence, where $\mathbb{E}_{\{\mathbf{h}\}}\{\cdot\}$ denotes the expectation with respect to the channel and noise realizations.

Since the CPU has no prior information of $\{\delta_{k'}\}$ and $\{\hat{m}_{k'}\}$, it could only make the hypothesis based on the statistical information, i.e.,

$$\begin{aligned}\bar{\mathcal{Y}} &\triangleq \mathbb{E}\{\mathcal{Y}\} \overset{(b)}{=} \tau_i \rho_i \sum_{l=1}^{L} \beta_{kl} \\ &+ \tau_i \rho_i \epsilon \sum_{l=1}^{L} \sum_{k'=1, k' \neq k}^{K} \beta_{k'l} \left(\frac{\mathbb{E}\{\hat{m}_{k'}\}}{m}\right)^2 + L\sigma^2,\end{aligned} \tag{31}$$

where $\mathbb{E}\{\hat{m}_{k'}\} = \sum_{i=1}^{m-1} i \frac{C(m,i) C(\tau_i - m, m-i)}{C(\tau_i, m)}$ and (b) comes from the fact that $\mathbb{E}\{\delta_{k'}\} = \epsilon$. We denote by $\mathcal{H}_0$ the hypothesis that UE k is idle and $\mathcal{H}_1$ the hypothesis that UE k is active. Then two possibly obtained values of $\bar{\mathcal{Y}}$ are

$$\bar{\mathcal{Y}}\Big|_{\mathcal{H}_0} = \tau_i \rho_i \varepsilon \sum_{l=1}^{L} \sum_{k'=1, k' \neq k}^{K} \beta_{k'l} \left(\frac{\mathbb{E}\{\hat{m}_{k'}\}}{m}\right)^2 + L\sigma^2, \tag{32}$$

$$\begin{aligned}\bar{\mathcal{Y}}\Big|_{\mathcal{H}_1} &= \tau_i \rho_i \sum_{l=1}^{L} \beta_{kl} \\ &+ \tau_i \rho_i \varepsilon \sum_{l=1}^{L} \sum_{k'=1, k' \neq k}^{K} \beta_{k'l} \left(\frac{\mathbb{E}\{\hat{m}_{k'}\}}{m}\right)^2 + L\sigma^2.\end{aligned} \tag{33}$$

It is clear that $\bar{\mathcal{Y}}\big|_{\mathcal{H}_1} > \bar{\mathcal{Y}}\big|_{\mathcal{H}_0}$ always holds for $\rho_i > 0$. Therefore, the CPU can simply make the decision by comparing $\mathcal{Y}$ with $\bar{\mathcal{Y}}\big|_{\mathcal{H}_0}$, i.e., UE k is active if $\mathcal{Y} > \bar{\mathcal{Y}}\big|_{\mathcal{H}_0}$, and idle otherwise.

4.3 CNN-based approach

The UADNet uses varying window sizes of 3×3 multiple filters to capture the most valuable features and the highest value, for each convolutional layer's feature map. Taking the received identifiers tensor $\mathbf{R}_\phi$ as input, the UADNet is combined by pooling structure, several basic blocks, and classification layer. Among them, a basic block is composed of three main kinds of operations: "*Conv*", "*ReLU*" and "*BN*", which represents *Convolution*, *Rectified Linear Units* and *Batch Normalization*, respectively. In addition, the layers of basic blocks are combined with "*Conv+BN+ReLU*", "*Conv+ReLU*", "*Conv*" and "Down Sampling". Each convolutional layer has same number of employed multiple filters, and different filter represents different feature map.

As shown in Figure 2, UADNet consists

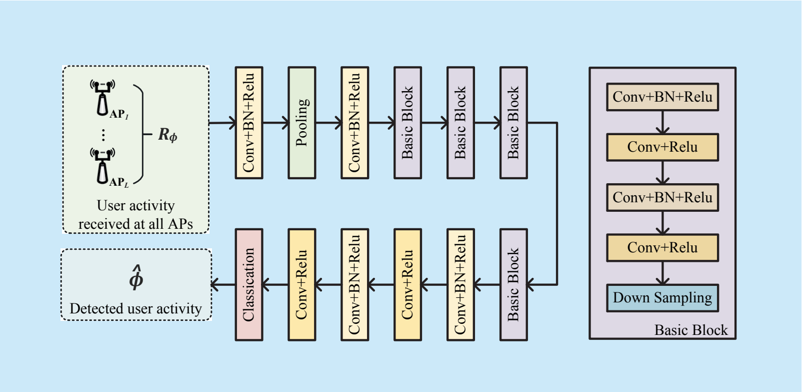

Fig. 2. *UADNet for non-orthogonal identifier sequences.*

of four basic blocks. Before going through the main body, the received identifiers tensor needs to be normalized. Through several basic blocks, with the powerful fitting ability, the convolutional neural network can detect the active user information hidden in the large-scale information of received signal. For the tail of UADNet, we use a fully connected layer to achieve classification function. The number of connection points of input and output for the last layer is $0.25\tau_i LD$ and K, respectively. Specifically, the UADNet is formulated as $\hat{\phi} = \mathcal{F}(\mathbf{R}_\phi, \Theta)$, where Θ represents the model parameters. The label $\hat{\phi}$ can be represented as a one-hot vector $e_k = [0,\ldots,0,1,0,\ldots,0]$, which is 1 at the k-th location, and 0 elsewhere.

Our baseline is a combination of a series CNN and fully connected deep neural network (DNN), which is similar to the several successful image classifiers. For each experiment, we coarsely optimize mini-bench and learning rate for the frame level classification accuracy.

For user activity detector scheme, the bottleneck of user detection is the high computational complexity. In our user detection method, the computational complexity include propagation for forward and backward. The computational complexity of the training phase is given by

$$\mathcal{O}\left(2st\tau_i L\left(\kappa^2\left(N_B + 2.25\right)D^2 + 0.25DK\right)\right), \quad (34)$$

where s donates the size of batch size, t donates the iterations number, κ^2 donates the kernels size. Additional, N_B and D denote the total number of basic block and the features for the convolutional layer of UADNet, respectively.

The average online detection time (in seconds) of UADNet could be ~ 0.1.

V. INITIAL ACCESS AND RESOURCE ALLOCATION

When UE k is detected to be active, it needs to access the system by being assigned system resources, i.e., a pilot for CE and serving APs for service. However, UE k cannot select its resources entirely freely since each AP only supports a limited number of UEs [18]. More precisely, each AP can only manage τ_p UEs, to avoid strong pilot contamination. Therefore, we adopt the following key assumption from [18].

Assumption 1. *Each AP serves at most one UE per pilot and uses all its N antennas to serve these UEs.*

The above assumption implies that $|\mathcal{D}_l| \leqslant \tau_p$.

In order to satisfy Assumption 1 and guarantee every UE is served by at least one AP, we develop a scheme jointly performing AP selection and pilot assignment based on a competitive mechanism. The intention is that UE k finds the pilot $\boldsymbol{\varphi}_t$ with minimum interference, meanwhile selects APs serving itself with $\boldsymbol{\varphi}_t$ as many as possible. Given that UE k' is already served by AP l with $\boldsymbol{\varphi}_t$, UE k needs to compete against UE k' for the service from AP l with $\boldsymbol{\varphi}_t$; we refer this pilot-AP pair as (t,l). UE k succeeds in the competition if UE k has better channel condition than UE k', i.e., $\beta_{kl} > \beta_{k'l}$. The lost UE (referred to as UE k^*) puts (t,l) into its *blacklist* $\mathcal{B}_{k^*} \subset \left\{(t,l): 1 \leqslant t \leqslant \tau_p, 1 \leqslant l \leqslant L\right\}$, which means the pilot-AP pair (t,l) is no longer available for UE k^*. This is reasonable since the UEs that have won the competition have better channel conditions than UE k^*, and thus UE k^* cannot win any competition regarding the pilot-AP pair (t,l). Moreover, if $|\mathcal{B}_{k^*}|$ reaches $\tau_p L - 1$, which means UE k^* has lost every competition it participated in, then UE k^* is added into the list $\mathcal{L}_{\overline{\mathrm{UE}}}$ and assigned to the only pilot-AP pair that is left; consequently, UE k^* no longer needs to participate in another competition. Since the transmission is sporadic, UE k^* is removed from $\mathcal{L}_{\overline{\mathrm{UE}}}$ when its transmission is finished. $\mathcal{L}_{\overline{\mathrm{UE}}}$ prevents the UEs in weak channel conditions from being abandoned. We denote by $\boldsymbol{\varphi}_k$ the pilot assigned to UE k and $\mathcal{L}_{\mathrm{UE}}$ the list comprising the active UEs which have not accessed the system yet. The algorithm initiates with $\mathcal{L}_{\mathrm{UE}} = \mathcal{K}$, $\mathcal{L}_{\overline{\mathrm{UE}}} = \varnothing$, $\{\mathcal{M}_k = \varnothing : k \in \mathcal{K}\}$, $\{\mathcal{B}_k = \varnothing : k \in \mathcal{K}\}$, and $\{\boldsymbol{\varphi}_k = \mathbf{0} : k \in \mathcal{K}\}$.

Our proposed scheme operates through the following steps.

1) UE $k = [\mathcal{L}_{\mathrm{UE}}]_1$ measures $\mathrm{tr}(\boldsymbol{\Psi}_{tl})/\beta_{kl}$ for all available pilot-AP pairs.

2) UE k finds pilot

$$t = \arg\min_{(t,l)\in\mathcal{P}/\mathcal{B}_k} \mathrm{tr}(\boldsymbol{\Psi}_{tl})/\beta_{kl}, \tag{34}$$

where $\mathcal{P} = \{(t,l) : 1 \leqslant t \leqslant \tau_p, 1 \leqslant l \leqslant L\}$.

If AP l serves no UE with $\boldsymbol{\varphi}_t$, then $\boldsymbol{\varphi}_t$ is assigned to UE k, AP l is selected into $\mathcal{M}_k$, and UE k repeats Step 4) for more possible serving APs; otherwise, a competition between for sharing $\boldsymbol{\varphi}_t$ is needed, which is elaborated in Step 3).

3) A competition for sharing $\boldsymbol{\varphi}_t$ occurs when UE k attempts to select pilot-AP pair (t,l) while AP l has already served a UE k' with $\boldsymbol{\varphi}_t$. The principle is that AP l gives priority to the UE with better channel condition. Therefore, if $\beta_{kl} > \beta_{k'l}$, then $\boldsymbol{\varphi}_t$ is assigned to UE k, with which AP l turns to serve UE k, UE k' puts (t,l) into $\mathcal{B}_{k'}$, and UE k repeats Step 4) for more possible serving APs; otherwise, UE k puts (t,l) into $\mathcal{B}_k$ and repeats Step 2) for another available pilot, until $k \in \mathcal{L}_{\overline{\mathrm{UE}}}$. In the case of $k \in \mathcal{L}_{\overline{\mathrm{UE}}}$, UE k selects whatever (t,l) left in $\mathcal{P}/\mathcal{B}_k$. By then, UE k finishes its AP selection and is moved from $\mathcal{L}_{\mathrm{UE}}$.

4) Competitions for more serving APs between UE k and the UEs in $\mathcal{S}_t$ occur after $\boldsymbol{\varphi}_t$ is assigned to UE k. Similar to Step 3), APs give priority to the UEs with better channel conditions. Therefore, for UE $k' \in \mathcal{S}_t$, which is served by AP l, if $\beta_{kl} > \beta_{k'l}$, then AP l turns to serve UE k and UE k' puts (t,l) into $\mathcal{B}_{k'}$; otherwise, UE k puts (t,l) into $\mathcal{B}_k$.

By then, UE k accesses the system and therefore is moved from $\mathcal{L}_{\mathrm{UE}}$.

5) Go back to Step 1) for the next UE, until $\mathcal{L}_{\mathrm{UE}} = \varnothing$.

The pseudo code of this algorithm is given in Algorithm 1.

Algorithm 1. Joint AP selection and pilot assignment.

Input: $\mathcal{P}, \mathcal{L}_{\mathrm{UE}}, \mathcal{L}_{\overline{\mathrm{UE}}}, \{\mathcal{M}_k\}, \{\mathcal{B}_k\}$
Output: $\{\mathcal{M}_k\}, \{\boldsymbol{\varphi}_k\}$
for $k \in \mathcal{L}_{\mathrm{UE}}$ **do**
  repeat
    $\bar{\mathcal{M}}_k = \{(t,l) : l \in \mathcal{M}_k\}$;
    $\mathcal{P}_k \leftarrow \mathcal{P}/\{\bar{\mathcal{M}}_k \cup \mathcal{B}_k\}$;
    if $\mathcal{P}_k = \varnothing$ **then**
      break;
    if $k \in \mathcal{L}_{\overline{\mathrm{UE}}}$ **then**
      $\{(t', l')\} = \mathcal{P}_k$;
      $\boldsymbol{\varphi}_k \leftarrow \boldsymbol{\varphi}_{t'}$;
      $\mathcal{M}_k \leftarrow \{l'\}$;
    break;
    else
      If $\boldsymbol{\varphi}_k = \mathbf{0}$ **then**
        // Competition for pilot
        $(t,l) = \arg\min_{(s,j)\in\mathcal{P}/\mathcal{B}_k} \mathbf{tr}(\boldsymbol{\Psi}_{sj})/\beta_{kj}$;
      else
        // Competition for pilot
        $l = \arg\min_j \mathbf{tr}(\boldsymbol{\Psi}_{tj})/\beta_{kj}$;
      $\mathcal{M}_k \leftarrow \mathcal{M}_k \cup \{l\}$;
      If *AP l serves a UE k' with* $\boldsymbol{\varphi}_k = \mathbf{0}$ **then**
        $k^* = \arg\min_{i\in\{k,k'\}/\mathcal{L}_{\overline{\mathrm{UE}}}} \beta_{ij}$;
        If $k^* \neq k$ **then**
          $\boldsymbol{\varphi}_k \leftarrow \boldsymbol{\varphi}_{t'}$;
          $\mathcal{B}_{k^*} \leftarrow \mathcal{B}_{k^*} \cup \{(t,l)\}$;
          If $|\mathcal{B}_{k^*}| \leftarrow \tau_p L - 1$ **then**
            $\mathcal{L}_{\overline{\mathrm{UE}}} \leftarrow \mathcal{L}_{\overline{\mathrm{UE}}} \cup \{k^*\}$;
          $\mathcal{M}_{k^*} \leftarrow \mathcal{M}_{k^*}/\{l\}$;
Until break;

VI. NUMERICAL EVALUATION

We consider a setup where L APs and $K \sim 10^4$ UEs are independently and uniformly distributed in a 50×50 m^2 square coverage area. All APs are equipped with half-wavelength-spaced uniform linear arrays with N antennas. Unless specified, $L = 100$, $N = 8$, and the number of the active UEs $|\mathcal{K}| = 20$, which implies $\epsilon = 0.01$ when $K = 2000$. We apply the wrap-around technique to mimic an infinitely large network with 8000 active UEs/km^2.

The 3GPP Urban Microcell model in [40, Tab. B.1.2.1-1] is used to compute the large-scale propagation conditions, such as pathloss and shadow fading. Beyond that, we refer to system setup parameters in [33], [34], where the noise variance is $\sigma^2 = -92$ dBm, the uplink pilot transmit power $\rho_p = -40$ dBm, the maximum downlink transmit power is $\rho_d = 5$ W, the RF-to-DC conversion efficiency is $\xi = 0.3$, the bandwidth is 20 MHz, the coherence blocks contain $\tau_c = 200$ channel uses, and the channel uses for pilot is $\tau_p = 10$. Unless specified, the time switch ratio $\lambda = 0.1$.

The simulations are performed in PyCharm Community Edition (Python 3.7 environment) on a computer with Intel Core i7-9700K CPU @ 3.6GHz, 32 GB of RAM and an Nvidia GeForce RTX 2080Ti GPU. The average running times (in seconds) of CNN is 0.114094.

We first evaluate our proposed UADNet and the benchmark (marked as "PWR" in Figure 3) with different identifier length of $\tau_i = 20, m = 3$ and $\tau_i = 50, m = 2$, which generate $C(20,3) = 1140$ and $C(50,2) = 1225$ unique identifiers, respectively. The performance of error probability is considered, which is defined as the probability of the errors occur during the detection. In Figure 3, the first observation is our proposed UADNet outperforms the benchmark in every simulation setting. Then we notice that the error probability reduces as the number of APs L increases for every case, which comes from the diversity gain of multiple APs. It can be seen in both detection methods that the detection accuracy is improved when the number of the active UEs $|\mathcal{K}|$ is relative small. The reason is the smaller $|\mathcal{K}|$ increases the probability that an active UE's identifier is orthogonal with the other active UEs. When comparing Figure 3(a) and Figure 3(b), we can see that the error probability is smaller when the identifier length of $\tau_i = 50, m = 2$ is selected instead of $\tau_i = 20, m = 3$, since the former has greater

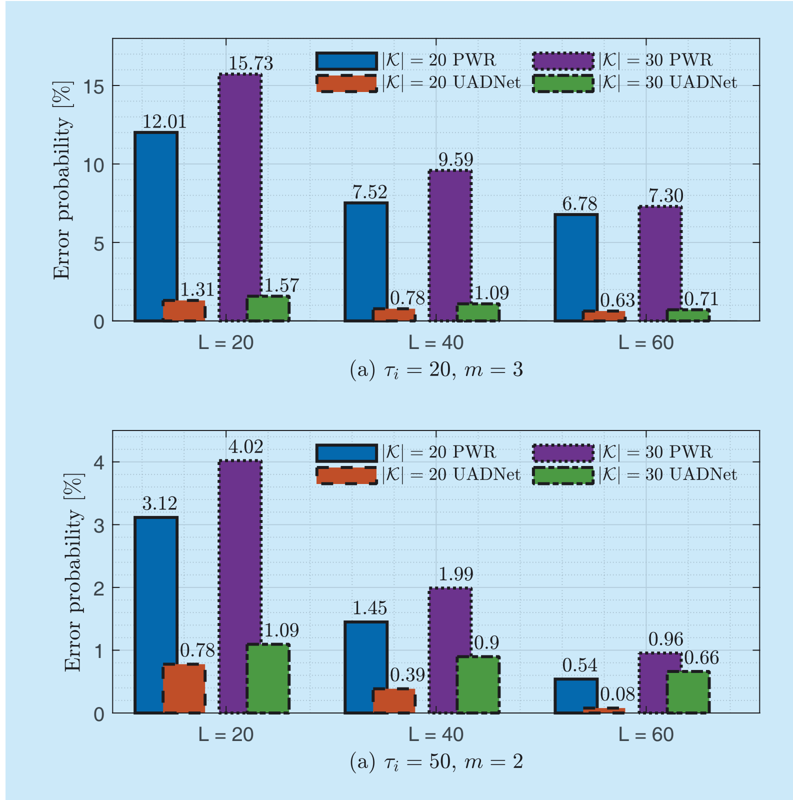

Fig. 3. *Error probability with different combinations of numbers of APs, numbers of active UEs, and identifier length.*

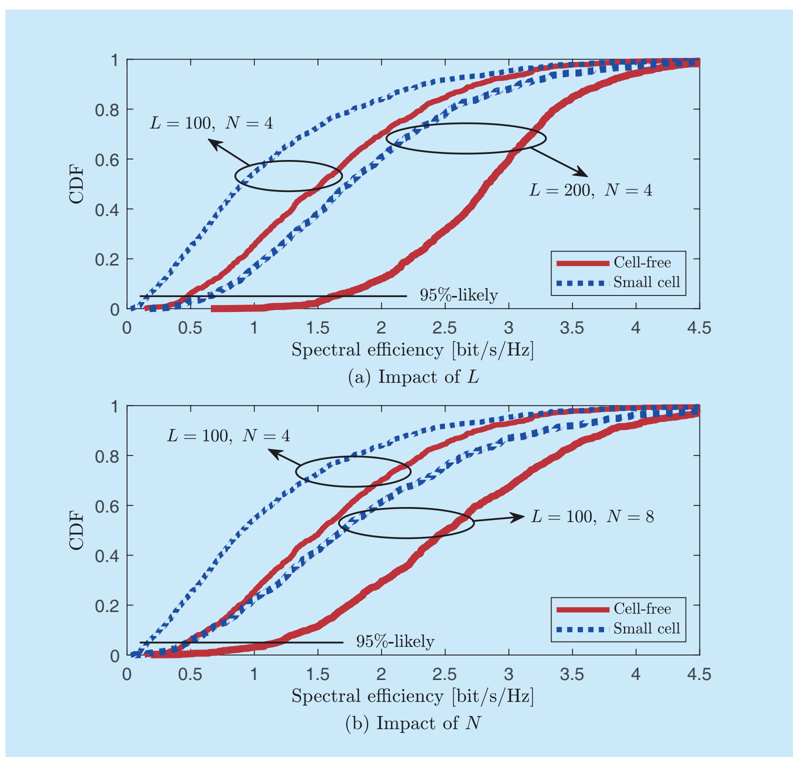

Fig. 4. *Comparison of cell-free and small cell on SE per UE with different combinations of numbers of APs and numbers of antennas per AP (LP-MMSE combining, $\theta = 1$, $\lambda = 0.1$).*

probability that an active UE's identifier is orthogonal with the other active UEs than the latter. That implies the performance of the UADNet could be further improved by designing a more delicate manner to construct the identifier sequences.

Then we demonstrate the advantage of the cell-free operation compared with the small cell operation on SE performance when the ESS IoE scenarios are considered. In small cell operation, the uplink signal from UE k is decoded by using only the received signal from one AP, which could be the one that maximizes the SE or the one with the largest large-scale fading coefficient. In this case, the signal processing can be dealt locally at the AP by using its own local CSI without exchange anything with the CPU. We refer to the small cell operation in [14] where a UE is only served by the AP which maximizes the SE, and treat it as a benchmark in our considered ESS IoE system. The proposed initial access scheme is applied in the following two figures.

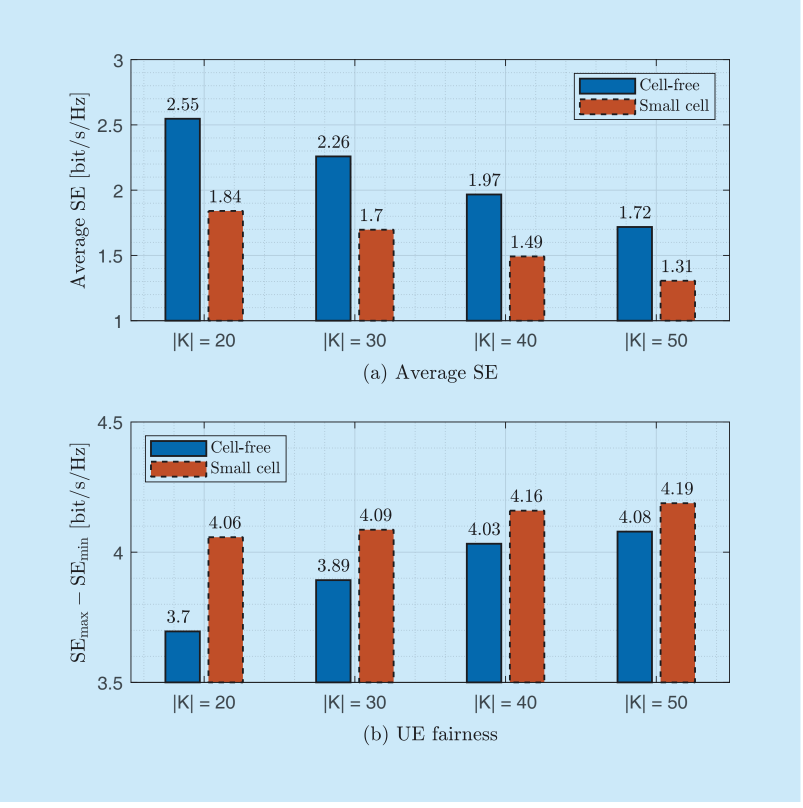

Fig. 5. *Comparison of cell-free and small cell on average SE and UE Fairness with different combinations of numbers of active UEs (LP-MMSE combining, $\theta = 1$, $\lambda = 0.1$).*

Figure 4 depicts the cumulative distribution function (CDF) of the SE per UE with LP-MMSE combining, power control factor $\theta = 1$, and time switch ratio $\lambda = 0.1$ for the setups of $(L, N) = (100, 4)$, $(200, 4)$, and $(100, 8)$, which are denoted as "case 1", "case 2", and "case 3", respectively. We compare the cell-free operation with small cell operation when the impact of number of APs L and the impact of the number of the antennas per AP N are considered. It can be observed from Figure 4 that the cell-free operation outperforms small cell in all three cases. More specifically, Compared with small cell, cell-free achieves 0.31 bit/s/Hz, 1.00 bit/s/Hz and 0.70 bit/s/Hz improvement in 95%-likely SE for the case 1, case 2, and case 3, respectively. When comparing Figure 4(a) and Figure 4(b), we notice that case 2 offers more improvement than case 3 compared with case 1, which implies that the number of APs L has more impact on the SE performance than the number of the antennas per AP N. The rationale behind this is the increased macro-diversity plays a dominant role in the considered IoE system; that is the average distance from a UE to an AP is reduced when the number of APs increases.

The average SE and UE fairness of the considered system are demonstrated through Figure 5, where the impact of the crowds in the system, i.e., the number of the active UEs $|\mathcal{K}|$ is considered with LP-MMSE combining, power control factor $\theta = 1$, and time switch ratio $\lambda = 0.1$ for the setup of $L = 100$ and $N = 8$. Note that the fairness is measured by the difference between the maximum and minimum values of the SE, i.e., $\mathrm{SE}_{\max} - \mathrm{SE}_{\min}$. When comparing cell-free and small cell, the general results are the same as in Figure 5 that cell-free outperforms small cell in terms of average SE and UE fairness. In Figure 5(a) we can see that the average SE of both cell-free and small cell reduces as the number of the active UEs $|\mathcal{K}|$ increases due to the increased inter-user interference. Moreover, we notice that the advantage of the cell-free compared with small cell on average SE gets less prominent when $|\mathcal{K}|$ gets larger, for instance 38.59% improvement when $|\mathcal{K}|=20$ and 31.30% improvement when $|\mathcal{K}|=50$. The reason is that the average distance from a UE to its nearest AP is increased when the system gets crowder, which makes the nearest AP seem more dominant and hence narrows the average SE gap between cell-free and small cell. In Figure 5(b) we can see that the UE fairness of both cell-free and small cell reduces as $|\mathcal{K}|$ increases due to Assumption 1; that is, a UE is served by less APs when the number of the active UEs increases.

Since we have demonstrated that cell-free operation outperforms small cell operation in the considered IoE system with LP-MMSE combining, the following results focus on the performance of the initial access scheme proposed in Section V with MR combining, the impacts of the time switch ratio λ and the power control factor θ, and the tightness of the closed-form expression of harvested energy provided in Lemma 2 and the closed-form expression of SE provided in Lemma 4. Figure 6 compares the proposed initial access scheme and the one proposed in [18], which is referred to as ``Scalable", in average SE by considering the impact of the time switch ratio λ with power control factor $\theta=0$ and $\theta=1$. The first observation is that the analytical results match the simulation very well. Then we notice the significant deteriorations in average SE when λ reaches either 0 or 1, due to the fact that the harvested energy turns either too small that a UE lacks sufficient power to train the pilot signal or transmit the payload data when $\lambda \to 0$, or needlessly too large that no time left for payload data transmission $\lambda \to 1$. Moreover, the proposed initial access scheme seems to offer better performance in average SE compared with Scalable, since the competition mechanism in the proposed scheme allows a UE to select as many serving APs as possible (under Assumption 1) and jointly considers the interference on one pilot sequence and the channel condition with an AP. When comparing Figure 5(a) and Figure 5(b), we notice that

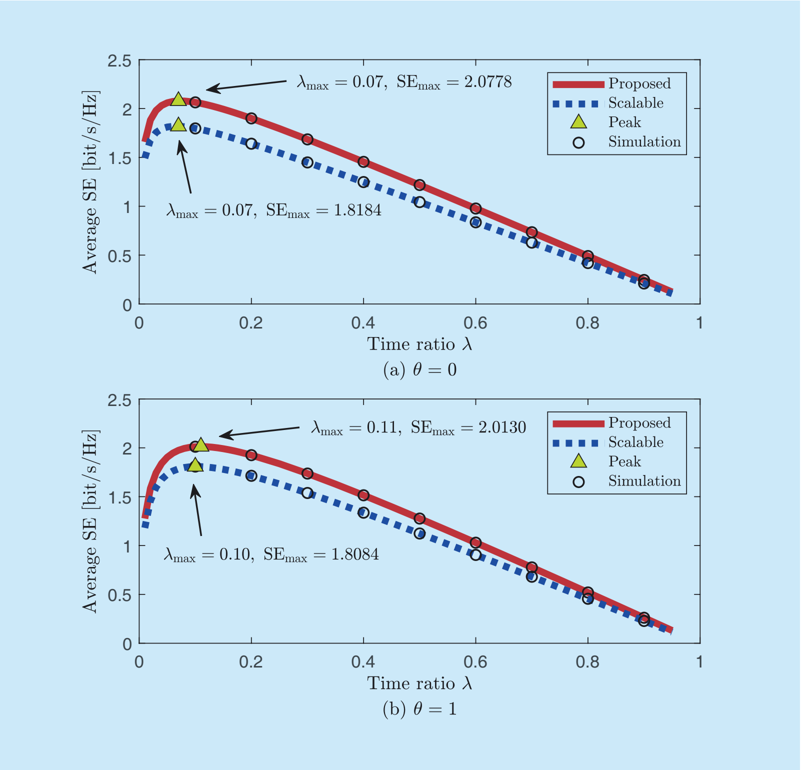

Fig. 6. *Average SE with different combinations of access schemes and time ratios (MR combining).*

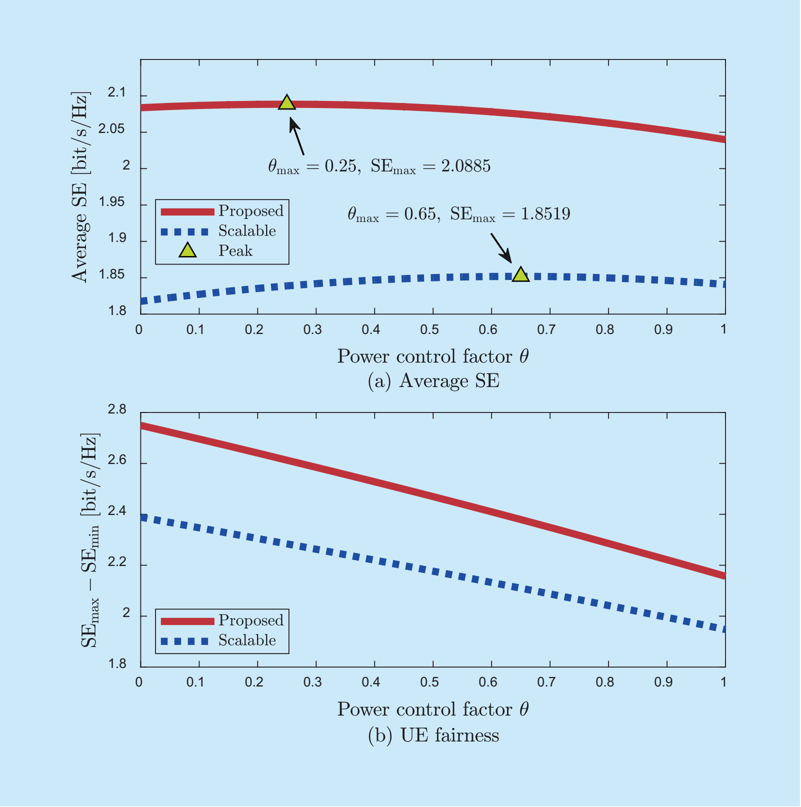

Fig. 7. *Average SE and Fairness with different combinations of access schemes and power control factors (MR combining, $\lambda=0.1$).*

the optimal λ with the maximum average SE in both schemes when $\theta = 1$ is larger than the one when $\theta = 0$, which implies that more energy is needed to achieve the maximum average SE when the UE fairness is given priority to. Moreover, case $\theta = 1$ loses in the maximum average SE in both schemes due to the trade-off between the SE performance and UE fairness, where $\theta = 1$ promotes more fairness.

Next, Figure 7 evaluates the proposed scalable power control policy on the average SE and UE fairness with considering with time switch ratio $\lambda = 0.1$. When comparing the proposed initial access scheme and Scalable, the general results are the same as in Figure 7 that proposed scheme outperforms Scalable in terms of average SE and UE fairness. In Figure 7 (a) we notice that the average SE is concave with respect to the power control factor θ instead of monotonically increasing as the uplink transmit power increases, i.e., $\theta \to 0$. The reason is that the inter-user interference increases, which deteriorates the SINR of the received data signal at APs, when all UEs exploit their full transmit power. It can be observed from Figure 7 (b) that larger values of θ promotes more fairness among the UEs. Since for a UE, the disadvantage on the large-scale fading coefficients between its serving APs will be compensated with the transmission power. According to (28), the compensation increases as the value of θ increases. Note that LP-MMSE combining outperforms MR combing by utilizing the CSI of the UEs served by one AP, which is a common view, hence the comparison of LP-MMSE combining and MR combining is not especially demonstrated. However, the advantage of the LP-MMSE combining can still be found when comparing Figure 5(a) and Figure 76(b), where LP-MMSE combining offers average SE of 2.55 bit/s/Hz while MR combining offers average SE of 2.01 bit/s/Hz with the setup of $|\mathcal{K}| = 20$, $\theta = 1$, and $\lambda = 0.1$.

VII. Conclusion

Supporting massive access with trivial performance loss on SE and UE fairness is the key to the scalable implementation of ESS IoE networks in 6G. In order to achieve that, we proposed a framework comprising a CNN-based user activity detector, an initial access scheme which jointly performs AP selection and pilot assignment, and a scalable power control policy considering both uplink and downlink. The bottleneck of the considered IoE networks, i.e., data decoding is deteriorated by the poor CSI which is led by the inappropriate pilot structure dedicated to massive access, was much relieved by decoupling the UE identifier and pilot sequences. The SE and UE fairness with LP-MMSE and MR combining was considered to evaluate our proposed framework, where the user and antenna density were taken into account. Two new closed-form expressions for harvested energy with MR precoding and SE with MR combining were derived.

The simulation results demonstrate that our proposed framework performs well compared with the state-of-the-art. Specifically, our proposed UADNet achieves an excellent detection performance with the error probability of 10^{-4} when considering non-orthogonal UE identifiers. Due to the strong diversity gain, cell-free operation outperforms the small cell on both SE and UE fairness, especially when the antenna density gets large. By jointly suppressing the inter-user interference and selecting the best serving APs, the proposed initial access scheme can offer 14.3% improvement on average SE compared with the benchmark. Moreover, the optimum SE performance can be achieved by adjusting the time allocation between the downlink energy harvest and the uplink data transmission. Finally, the proposed scalable power control provides the trade-off of the fairness among the users and the average SE.

This paper provides a feasible solution for massive access in ESS IoE CF mMIMO networks, which can be straightforwardly generalized the study of other important factors, such as energy efficiency, hardware impairment, limited fronthaul capacity, non-linear energy harvesting model, etc.

References

[1] B. Ai, A. F. Molisch *et al.*, "5G key technologies for smart railways," *Proceedings of the IEEE*, vol. 108, no. 6, 2020, pp. 856–893.

[2] W. Saad, M. Bennis *et al.*, "A vision of 6G wireless systems: Applications, trends, technologies, and open research problems," *IEEE network*, vol. 34, no. 3, 2019, pp. 134–142.

[3] K. B. Letaief, W. Chen *et al.*, "The roadmap to 6G: AI empowered wireless networks," *IEEE Communications Magazine*, vol. 57, no. 8, 2019, pp. 84–90.

[4] K. Xu, Y. Qu *et al.*, "A tutorial on the internet of things: From a heterogeneous network integration perspective," *IEEE network*, vol. 30, no. 2, 2016, pp. 102–108.

[5] J. Zhang, E. Björnson *et al.*, "Prospective multiple antenna technologies for beyond 5G," *IEEE Journal on Selected Areas in Communications*, vol. 38, no. 8, 2020, pp. 1637–1660.

[6] T. L. Marzetta, "Noncooperative cellular wireless with unlimited num- bers of base station antennas," *IEEE Transactions on Wireless Communications*, vol. 9, no. 11, 2010, pp. 3590–3600.

[7] E. G. Larsson, O. Edfors *et al.*, "Massive MIMO for next generation wireless systems," *IEEE Communications Magazine*, vol. 52, no. 2, 2014, p. 186–195.

[8] V. W. Wong, *Key technologies for 5G wireless systems*. Cambridge university press, 2017.

[9] H. Q. Ngo, A. Ashikhmin *et al.*, "Cell-free massive MIMO versus small cells," *IEEE Transactions on Wireless Communications*, vol. 16, no. 3, 2017, pp. 1834–1850.

[10] E. Nayebi, A. Ashikhmin *et al.*, "Precoding and power optimization in cell-free massive MIMO system- s," *IEEE Transactions on Wireless Communications*, vol. 16, no. 7, 2017, pp. 4445–4459.

[11] G. Interdonato, E. Björnson *et al.*, "Ubiquitous cell-free massive MIMO communications," *EURASIP Journal on Wireless Communications and Networking*, vol. 2019, no. 1, 2019, p. 197.

[12] J. Zhang, S. Chen *et al.*, "Cell-free massive MIMO: A new next-generation paradigm," *IEEE Access*, vol. 7, 2019, pp. 99878–99888.

[13] H. Q. Ngo, L.-N. Tran *et al.*, "On the total energy efficiency of cell-free massive MIMO," *IEEE Transactions on Green Communications and Networking*, vol. 2, no. 1, 2017, pp. 25–39.

[14] E. Björnson and L. Sanguinetti, "Making cell-free massive MIMO competitive with MMSE processing and centralized implementation," *IEEE Transactions on Wireless Communications*, vol. 19, no. 1, 2019, pp. 77–90.

[15] J. Zhang, Y. Wei *et al.*, "Performance analysis and power control of cell-free massive MIMO systems with hardware impairments," *IEEE Access*, vol. 6, 2018, pp. 55302–55314.

[16] J. Zheng, J. Zhang *et al.*, "Efficient receiver design for uplink cell-free massive MIMO with hardware impairments," *IEEE Transactions on Vehicular Technology*, vol. 69, no. 4, 2020, pp. 4537–4541.

[17] S. Buzzi and C. D'Andrea, "Cell-free massive MIMO: User-centric approach," *IEEE Wireless Communications Letters*, vol. 6, no. 6, 2017, pp. 706–709.

[18] E. Björnson and L. Sanguinetti, "Scalable cell-free massive MIMO systems," *IEEE Transactions on Communications*, vol. 68, no. 7, 2020, pp. 4247–4261.

[19] S. Chen, J. Zhang *et al.*, "Structured massive access for scalable cell-free massive MIMO systems," *IEEE Journal on Selected Areas in Communications*, early access, 2020.

[20] E. Björnson, J. Hoydis *et al.*, "Massive MIMO networks: Spectral, energy, and hardware efficiency," *Foundations and Trends® in Signal Processing*, vol. 11, no. 3-4, 2017, pp. 154–655.

[21] Y. Zeng, B. Clerckx *et al.*, "Communications and signals design for wireless power transmission," *IEEE Transactions on Communications*, vol. 65, no. 5, 2017, pp. 2264–2290.

[22] J. Hu, K. Yang *et al.*, "Integrated data and energy communication network: A comprehensive survey," *IEEE Communications Surveys & Tutorials*, vol. 20, no. 4, 2018, pp. 3169–3219.

[23] J. Hu, M. Li *et al.*, "Unary coding controlled simultaneous wireless information and power transfer," *IEEE Transactions on Wireless Communications*, vol. 19, no. 1, 2019, pp. 637–649.

[24] L. Zhao and X. Wang, "Massive MIMO downlink for wireless information and energy transfer with energy harvesting receivers," *IEEE Transactions on Communications*, vol. 67, no. 5, 2019, pp. 3309–3322.

[25] K. Senel and E. G. Larsson, "Grant-free massive MTC-enabled massive MIMO: A compressive sensing approach," *IEEE Transactions on Communications*, vol. 66, no. 12, 2018, pp. 6164–6175.

[26] E. De Carvalho, E. Björnson *et al.*, "Random pilot and data access in massive MIMO for machine-type communications," *IEEE Transactions on Wireless Communications*, vol. 16, no. 12, 2017, pp. 7703–7717.

[27] A. Fengler, G. Caire *et al.*, "Massive MIMO unsourced random access," CoRR, vol. abs/1901.00828, 2019. [Online]. Available: https://arxiv.org/abs/1901.00828.

[28] X. Chen, Z. Zhang *et al.*, "Fully non- orthogonal communication for massive access," *IEEE Transactions on Communications*, vol. 66, no. 4, 2017, pp. 1717–1731.

[29] X. Shao, X. Chen *et al.*, "A dimension reduction-based joint activity detection and channel estimation algorithm for massive access," *IEEE Transactions on Signal Processing*, vol. 68, 2019, pp. 420–435.

[30] L. Li, Z. Ma *et al.*, "Cutoff rate of sparse code multiple access in downlink broadcast channels," *IEEE Transactions on Communications*, vol. 65, no. 8, 2017, pp. 3328–3342.

[31] E. Nayebi, A. Ashikhmin *et al.*, "Performance of cell-free massive MIMO systems with MMSE and LSFD receivers," *in Proc. IEEE 50th Asilomar Conference on Signals*, Systems and Computers, 2016, pp. 203–207.

[32] R. Shrestha and G. Amarasuriya, "SWIPT in cell-free massive MIMO," *in Proc. IEEE Global Communications Conference*, 2018, pp. 1–7.

[33] X. Wang, A. Ashikhmin *et al.*, "Wirelessly powered cell-free IoT: Analysis and optimization," *IEEE Internet of Things Journal*, to appear, 2020.

[34] Ö. T. Demir and E. Björnson, "Joint power control and LSFD for wireless-powered cell-free massive MIMO," CoRR, vol abs/2002.09270, 2020. [Online]. Available: https://arxiv.org/abs/2002.09270.

[35] H. Liu, J. Zhang *et al.*, "Tabu- search based pilot assignment for cell-free massive mimo systems," *IEEE Transactions on Vehicular Technology*, vol. 69, no. 2, 2020, pp. 2286–2290.

[36] H. Liu, J. Zhang *et al.*, "Graph coloring based pilot assignment for cell-free massive MIMO systems," *IEEE Transactions on Vehicular Technology*, vol. 69, no. 8, 2020, pp. 9180–9184.

[37] L. Liu and W. Yu, "Massive connectivity with massive MIMO-Part I: Device activity detection and channel estimation," *IEEE Transactions on Signal Processing*, vol. 66, no. 11, pp. 2933–2946, Nov. 2018.

[38] Y. Jin, J. Zhang, S. Jin, and B. Ai, "Channel estimation for cell-free mmwave massive MIMO through deep learning," *IEEE Transactions on Vehicular Technology*, vol. 68, no. 10, pp. 10325–10329, Oct. 2019.

[39] Y. Jin, J. Zhang, B. Ai, and X. Zhang, "Channel estimation for mmwave massive MIMO with convolutional blind denoising network," *IEEE Communications Letters*, vol. 24, no. 1, pp. 95–98, Jan. 2020.

[40] 3GPP, "Further advancements for E-UTRA physical layer aspects (re- lease 9)," *3GPP TS 36.814*, Mar. 2017.

Biographies

Shuaifei Chen, received his B.S. degree in communication engineering from Beijing Jiaotong University, China, in 2018. From 2018, he is a PhD student in Beijing Jiaotong University. His research interests include massive MIMO systems and machine learning for signal processing in communications.

Jiayi Zhang (S'08-M'14-SM'20), received the B.Sc. and Ph.D. degree of Communication Engineering from Beijing Jiaotong University, China in 2007 and 2014, respectively. Since 2016, he has been a Professor with School of Electronic and Information Engineering, Beijing Jiaotong University, China. From 2014 to 2016, he was a Postdoctoral Research Associate with the Department of Electronic Engineering, Tsinghua University, China. From 2014 to 2015, he was also a Humboldt Research Fellow in Institute for Digital Communications, Friedrich-Alexander-University Erlangen-Nürnberg (FAU), Germany. From 2012 to 2013, he was a visiting scholar at the Wireless Group, University of Southampton, United Kingdom. His current research interests include cell-free massive MIMO, reconfigurable intelligent surface, communication theory and applied mathematics. Dr. Zhang received the Best Paper Awards at the WCSP 2017 and IEEE APCC 2017. He was recognized as an exemplary reviewer of the IEEE Communications Letters in 2015-2017. He was also recognized as an exemplary reviewer of the IEEE Transactions on Communications in 2017-2019. He was the Lead Guest Editor of the special issue on ``Multiple Antenna Technologies for Beyond 5G" of the IEEE Journal on Selected Areas in Communications in 2020. He currently serves as an Associate Editor for IEEE Transactions on Communications, IEEE Communications Letters, IEEE Access and IET Communications.

Yu Jin, received his B.S. degree in communication engineering from Beijing Jiaotong University, China, in 2019. From 2019, he is a Master student in Beijing Jiaotong University. His research interests include massive MIMO systems and machine learning for signal processing in communications.

Bo Ai (M'00-SM'10), received his Master degree and Ph. D. degree from Xidian University in China. He graduated from Tsinghua University with the honor of Excellent Postdoctoral Research Fellow at Tsinghua University in 2007. He was a visiting professor at EE Department, Stanford University in 2015. He is now working at Beijing Jiaotong University as a full professor and Ph. D. candidate advisor. He is the Deputy Director of State Key Lab of Rail Traffic Control and Safety, and the Deputy Director of International Joint Research Center. He is one of the main responsible people for Beijing ``Urban rail operation control system" International Science and Technology Cooperation Base, and the backbone member of the Innovative Engineering Based jointly granted by Chinese Ministry of Education and the State Administration of Foreign Experts Affairs. He has authored/co-authored 8 books and published over 300 academic research papers in his research area. He has hold 26 invention patents. He has been the research team leader for 26 national projects and has won some important scientific research prizes. Five papers have been the ESI highly-cited paper. He has been notified by Council of Canadian Academies (CCA) that, based on Scopus database, Prof. Bo Ai has been listed as one of the Top 1% authors in his field all over the world. Prof. Bo Ai has also been Feature Interviewed by IET Electronics Letters. His interests include the research and applications of channel measurement and channel modeling, dedicated mobile communications for rail traffic systems. Prof. Bo Ai is a Fellow of the Institution of Engineering and Technology (IET Fellow), IEEE VTS Distinguished Lecturer. He is an IEEE VTS Beijing Chapter Vice Chair. IEEE BTS Xi'an Chapter Chair. He was as a Co-chair or a Session/Track Chair for many international conferences. He is an associate editor of IEEE Antennas and Wireless Propagation Letters, IEEE Transactions on Consumer Electronics and an Editorial Committee Member of the Wireless Personal Communications journal. He is the Lead Guest Editor for Special Issues on IEEE Transactions on Vehicular Technology, IEEE Antennas and Propagations Letters, International Journal on Antennas and Propagations. He has received many awards such as Distinguished Youth Foundation and Excellent Youth Foundation from National Natural Science Foundation of China, the Qiushi Outstanding Youth Award by Hong Kong Qiushi Foundation, the New Century Talents by the Chinese Ministry of Education, the Zhan Tianyou Railway Science and Technology Award by the Chinese Ministry of Railways, and the Science and Technology New Star by the Beijing Municipal Science and Technology Commission.